Proceedings of the 2011 IEEE
International Conference on Robotics and Biomimetics
December 7-11, 2011, Phuket, Thailand

# Haptic Feature Extraction from a Biomimetic Tactile Sensor: Force, Contact Location and Curvature

Nicholas Wettels, *Member, IEEE* and Gerald E. Loeb, *Member, IEEE*

***Abstract*—The BioTac® is a biomimetic tactile sensor for grip control and object characterization. It has three sensing modalities: thermal flux, microvibration and force. In this paper, we discuss feature extraction and interpretation of the force modality data. The data produced by this force sensing modality during sensor-object interaction are monotonic but non-linear. Algorithms and machine learning techniques were developed and validated for extracting the radius of curvature (ROC), point of application of force (PAF) and force vector (FV). These features have varying degrees of usefulness in extracting object properties using only cutaneous information; most robots can also provide the equivalent of proprioceptive sensing. For example, PAF and ROC is useful for extracting contact points for grasp and object shape as the finger depresses and moves along an object; magnitude of FV is useful in evaluating compliance from reaction forces when a finger is pushed into an object at a given velocity while direction is important for maintaining stable grip.**

**Keywords - Biomimetic. Feature extraction, Haptics, Tactile sensors**

## I. Introduction

COMMERCIAL, linear force transducers usually have a "hockey-stick" input-output relationship: the output is saturated at a low (typically zero) value for inputs below a threshold, then increases linearly over its operating range until the output saturates at a high value for larger input signals. The manufacturer tailors the linear range of its products based on their specific applications. In the case of biological sensors, the hockey-stick relationship is replaced with a sigmoidal one that spans several decades. There is no evidence that the brain inverts this relationship expressly to compute the input signal (e.g. Newtons by the fingertips, lumens by the eyes). While it is obviously important for this information to be encoded by the system, the biological systems appear to use the embedded information directly in some fashion based on the task.

In this paper, we consider a biomimetic tactile sensor called a BioTac®, whose *non-linear* but wide dynamic ranges of multimodal sensing (Table 1) have been described in [8], [15] and at http://www.syntouchllc.com/home.htm. How should its data be processed? Should its outputs be linearized using machine learning and/ or curve-fitting techniques so they can be employed as commercial sensors, or is there a solution akin to biological systems? To make the best use of biomimetic sensors, it may be necessary to develop biomimetic signal processing in which neural networks directly adjust grip forces or decide on the identity of objects based on cognitive integration of Bayesian prior probabilities, well-chosen exploratory movements and multimodal sensory data. Furthermore, information from sensing modalities such as thermal flux (such as the human fingertip) may require information about contact location and forces to be interpretable. For example, information about the material composition of an object can be inferred from the rate of heat transfer from a heated finger to the object, but only if the location and force of contact are well-controlled and known.

Manuscript received July 21st, 2011. This material is based upon work supported by the National Science Foundation under Grant No. 0912260 Any opinions, findings, and conclusions or recommendations expressed in this material are those of the authors) and do not necessarily reflect the views of the National Science Foundation. Nicholas Wettels (email: nick.wettels@syntouchllc.com; phone 1-213-477-0710), and Gerald Loeb (email: gloeb@usc.edu) are with SynTouch LLC, Los Angeles, CA 90007 USA and the University of Southern California.

Table 1: BioTac Sensor Performance Characteristics

| Modality | Range | Frequency Response |
|---|---|---|
| Force | 0.01 – 50 N | 0 – 50 Hz |
| Microvibration | 0 – 2.0 kPa | 0 – 2000 Hz |
| Thermal Flux | 0 – 1.0 C/s | 0.1 – 50 Hz |

We report here on methods to linearize the outputs to show that force vectors and other canonical information are, in fact, embedded in the BioTac signals for two reasons: 1) it is important to demonstrate that the BioTac signals actually contain such information. 2) Early adopters of this technology will likely attempt to use the BioTac in lieu of conventional, linear sensors. Our goal and primary contribution is to extract tactile information with dynamic range and accuracy similar to humans, including: point of application of force (PAF), force vector (FV) and radius of curvature (ROC) (Table 2).

Table 2: Reasons for Extracting Haptic Properties

| Feature | Motivation for Extraction |
|---|---|
| Tri-axial Forces | - "Calibrating" other sensing modalities: e.g. thermal and microvibration [1]<br>- Force-cone based grip strategies [2,3]<br>- Evaluating object compliance |
| Point of Application of Force | - Calculating gripping points<br>- Contour following/ local shape<br>- Improving machine learning to estimate force |
| Radius of Curvature | - Determining global object shape<br>- Improving machine learning to estimate force |

The features listed in Table 2 have varying degrees of utility in extracting object properties using only cutaneous information from the sensors; in practice, their signals will generally be integrated with additional sensing from the robot itself such as joint angles, velocities and torques. For example, FV is useful in evaluating compliance from

reaction forces as a finger is depressed into an object at a given joint angle velocity. With regard to "calibration" of other sensing modalities for thermal sensing, we mean that normal forces affect the surface area and distance between the contacted object and the thermistor and thus the heat-flux. For texture and slip sensing, the force vector affects spectral content of the vibration signals.

Extracting features from tactile data using machine learning has been done before [4-7]. Here we show that calculating center of pressure and radius of curvature first aids in subsequent force vector calculation. For forces normal to an electrode, there is a monotonic increase in electrode impedance; the slopes of the curves depend complexly on probe curvature [8]. Other teams are working on related problems such as building tactile images for shape via object features [9-10] using tactile information for object grip and manipulation [5, 11-12].

## II. Methods

### A. Data Collection

The machine learning algorithms (MLA) were trained and then validated using data obtained from a BioTac sensor. The tactile sensor was secured facing upwards in a vise positioned on a 6-axis Advanced Mechanical Technology Inc. HE6x6-16 force-plate (Fig. 1). It was then exposed to probes with various radii of curvature that were used to generate various force vectors at various points of contact. Force directions were defined in the following manner: $F_z$ is vertical (downward = positive), $F_y$ is lateral (left = positive), and $F_x$ is along the longitudinal axis (towards the base of the vise = positive); see diagram. The digital protractor ensured the vise was level. The data were collected using a NI USB-SPI/I2C-8451 data acquisition block in conjunction with LabVIEW at 100 samples/s from all BioTac sensors and the force plate. All data collected were digitally filtered by a 3-pole, 5 Hz low-pass filter.

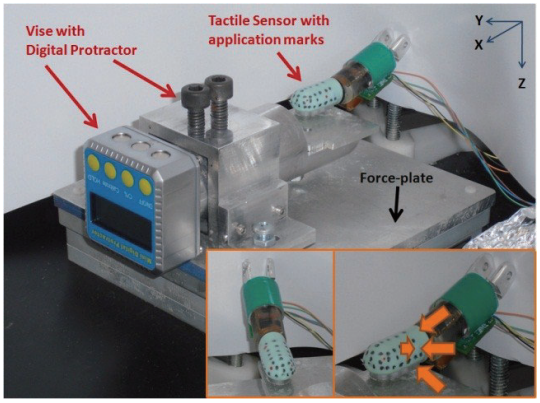


Figure 1: Data collection assembly with BioTac mounted to vise. Inset Lower Right: Orange arrows highlight force vectors applied (4 of 5 illustrated); metal adapter on proximal end of sensor attaches to Robonaut 2 hand system).

The data set involved manually stimulating the sensor along several application points via probes with various radii of curvature (Fig. 2).

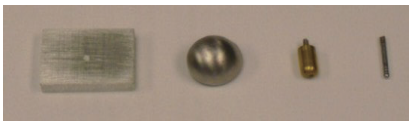

Figure 2: Various probes used to contact BioTac, from left to right: flat, 10mm, 3.6mm and 1mm radius of curvature

Probes were manually held with the hand steadied atop a solid block level with the vise. Contact was made normal to the surface of the skin and force increased to 30 - 40N. The force was relaxed, contact retained and the probe tilted approximately +/-30 degrees in each the X and Y plane (see Fig. 1, inset) then the motion repeated for a total of 5 stimulations. Stimulation motions were sufficiently slow relative to sample rate (100Hz) to assume quasi-static loading and care was taken to eliminate inadvertent dynamic events (e.g. probe slippage along the sensor surface). The small amount of tremor and variability from manual probing seemed to better represent realistic interactions and did not affect the accuracy of the force-plate data used for training and validation.

### B. Radius of Curvature

To extract ROC, a three-layer back-propagation perceptron classifier was used because it is capable of approximating any given nonlinear relation when a sufficient number of neurons are provided in the hidden layer [13]. Our goal was gross classification of ROC to determine its impact on FV, so sensitivity of ROC was not determined. MATLAB's Neural Network Toolbox 6.0.4 was used for classification; data for each voltage channel were preprocessed by subtracting the mean and dividing by the variance. Three-layer perceptron ANNs were created in MATLAB.

The basic mathematical structure of the ANN is a series of functional transformations. First we construct a linear combination of D input variables (Eqn. 1):

$$Aj = \sum_{i=1}^{D} WjiXi + Wj0 \qquad (1)$$

where parameters Wji refer to the weights and Wj0 refers to the biases of the activation function Aj. Each of these activation functions are transformed using a differentiable, non-linear function:

$$Zj = H(Aj) \qquad (2)$$

These M basis function outputs, referred to the hidden units, are linearly combined to form the K outputs for which the system was trained:

$$Ak = \sum_{j=1}^{M} WkjZj + Wk0 \qquad (3)$$

The Neural Network Toolbox employed the Levenberg-Marquardt back-propagation algorithm to tune the weights and biases of the ANN to maximize the correlation between the model predictions and the recorded data. Hidden units used hyperbolic tangent activation functions; outer units used linear functions. Hidden layer size was such that an adequate number of units existed relative to the inputs (2x inputs [14]). Overfitting was managed by using early

stopping and Bayesian regularization. Bayesian regularization maximizes the posterior probability of the weights and biases over an error function based on the training data. Early stopping examines the performance of the ANN during training in comparison to a novel validation data set. If the network's performance on the test set is no longer improved over five iterations, then training is stopped.

Prior to artificial neural network (ANN) training, the primary data sets were divided into three sets: 1) a working set (70%), with which the ANN was trained via back-propagation; 2) a validation set consisting of 15% of randomly chosen data to prevent overfitting; and 3) a test set of 15% randomly chosen data used to measure the ANN's ability to generalize after training. A confusion matrix was produced to show false positive and false negative misclassifications of the test set to evaluate network performance.

### C. *Point of Application of Force*

A 2-D coordinate system for PAF was generated based on the geometric pattern of fingerprints molded onto the contact surface of the BioTac skin (Figure 3). The fingerprints run the length of the skin and the coordinate "d" annotates the distance distalward from the proximal edge of the fingerprint pattern. The coordinate "r" denotes the radial distance from the centerline of the device; positions to the left from the ventral view in Figure 3 are negative. Compression of the skin normal to the surface (< 1mm) is relatively small compared to the span of stimulation points (4 to 8mm depending on probe) explored so positions were not corrected for this third dimension. This coordinate frame becomes polar as the fingerprints begin to curve over the convex fingertip because the "d" and "r" reference still uniquely define a location on the surface (Fig. 3).

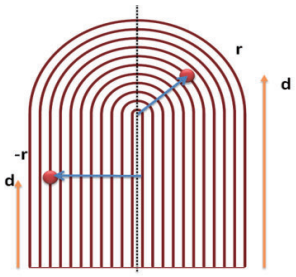


Figure 3: Illustration of the coordinate system of flattened skin as seen from the ventral surface; two sample points indicated in red.

Three "semi-rings" of stimulation points were chosen to probe the sensor, as shown in Fig. 1 and insets. One ring lay near the nail, another ran along the ventral centerline of the sensor and a third was approximately 4.5 mm between the two. Stimulation points started at the back of the sensor and occurred at approximately 4mm intervals. The two smaller probes were used for all PAFs, whereas the 10mm probe used every other point and omitted the intermediate ring entirely. The flat probe was used to generate FVs on each available plane of action (Z (towards ventral surface), X (towards tip), +/-Y (either lateral side)) as well as 45 degree intermediates. Total number of stimulations (5 vectors per points) for each probe was: 1mm: 95; 3.6mm: 95; 10mm: 65; flat: 35. Each 5-vector stimulation was saved as an individual file and then later merged to form a complete data set. Based on previous experiments showing impedance changes from probing about an electrode (Fig. 4), PAF determination should be tractable [8].

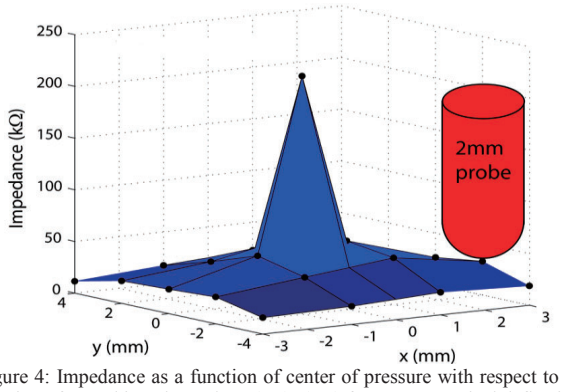


Figure 4: Impedance as a function of center of pressure with respect to the location of a working electrode at (x,y)=(0,0) for 4.5mm vertical deflections with a 2mm diameter probe. The sensor was systematically probed in a 4x5 grid (reproduced from [8]).

To calculate PAF, an interpolative look-up table was created based on the centers of the electrodes distributed over the core of the sensor. Because an increase in pressure results in a decrease in voltage from the sensor, electrode voltages were converted to force approximations (eqn.4) based on stimulation of an electrode with a 1mm ROC probe using a linear function (Eq. 4; R-squared = 0.9615); base-line voltages (V0) were subtracted to remove any drift bias.

$$Fest. = \frac{6.083}{(V - V0) + 1.976} \tag{4}$$

The three greatest approximated force levels were taken to "triangulate" the center of pressure. The corresponding positions of the three electrodes were used for a weighted average calculation based upon their respective force levels (eqn. 5).

$$PAF = \frac{P1 * Fest1 + P2 * Fest2 + P3 * Fest3}{\sum Ftot} \tag{5}$$

Thus an electrode with more force applied than another will bias the center of pressure towards that electrode. The estimated forces used for this weighting are not particularly accurate, but this has little effect on the position calculation because position determination is performed via look-up table based on ranking of force levels. Simultaneous contacts at multiple points could be resolved by altering the look-up table to search for multiple centers of pressure. For example, adjacent clusters of electrodes could be compared against one another to resolve multiple points of contact, but this is beyond the scope of this work. Errors in this system may occur at very low force levels when the sensor is not yet able to distinguish point of contact accurately. This problem can be mitigated by dynamically adjusting force thresholds of detection, smoothing noisy signals or both. Here, an 11-point robust Lowess moving average filter was used to

smooth the data. Given the dynamics of the system and sample rate of 100Hz, 11-point filtering would not result in significant lag if implemented in real-time. The robust Lowess filter uses weighted linear least squares and local linear regression to smooth the function; it also assigns zero weight to data points outside six standard deviations in its history.

### D. Force Vector

We have previously shown that as the skin deforms above a given working electrode, it constricts the flow path for ions between the electrode and ground, increasing electrode impedance [8]. The BioTac actually detects a voltage related nonlinearly to the conductance at each electrode, so voltage decreases with increasing force. This behavior has been characterized for forces normal to the plane of a single electrode [8]; we here examine how the entire population of electrodes can be used to encode tri-axial force vectors exerted on the BioTac. Calibration and zeroing of the sensor data are not considered in this work.

In Fig. 5, two different vectors consisting of normal and tangential forces are exerted on the sensor. In the case of Object A, the fluid bulges over the left and constricts over the right electrodes, resulting in asymmetric sensor voltage that can be related to the tangential force component by machine learning techniques. However, this behavior is non-linear and also depends on the point of application of force as well as the radius of curvature of the incident object [8].

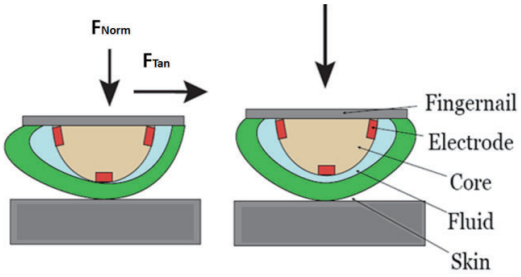


Figure 5: Cross-sectional view of distal phalanx of sensor; (Right) only normal force is applied to right object causing equal fluid displacement on both sides of sensor; (Left) large tangential-to-normal force ratio is exerted on object causing fluid to bulge and constrict over lateral electrodes on each side, respectively.

#### D1. Machine Learning Algorithms

Several variables must be considered when choosing a proper machine learning algorithm: number of free variables, computational efficiency and reliability and robustness over the problem set. In previous work [15], various time-domain filters (such as Kalman and particle filters) and kernel machines (Gaussian Mixture Model/Gaussian Mixture Regression, Gaussian Processes, Support Vector Machines and ANNs) were all considered for feature extraction. Results indicated ANNs were best suited to extracting features from the BioTac. ANNs are a well characterized machine learning technique and the software (Neural Network Toolbox 6.0.4) is well supported by Mathworks. The ANN used here is the similar to the previously mentioned classifier architecture except the output units use a linear output function and outputs were preprocessed only by subtracting their means.

#### D2. Feature Extraction/ Dimensionality Reduction

##### D2.1. Unsupervised

Two unsupervised feature extraction techniques were compared. The first was PCA; this was performed on the data and only components contributing >0.1% variance were kept. This operation was performed in MATLAB after preprocessing. The other unsupervised technique examined was independent components analysis (ICA). ICA differs from PCA in that the statistically independent components no longer need be uncorrelated. The FastICA v2.5 package (default setting) in MATLAB [16] was used to process the data. Both unsupervised and supervised methods were applied to the inputs of the machine learning algorithm, both to enhance features and also to reduce the number of inputs to simplify the machine learning process.

##### D2.2. Supervised

This single method attempts to simplify the feature extraction problem for the MLA by using a filter to remove those electrode inputs that do not correlate with forces [17]. A filter was created by analyzing electrode response versus forces over the wrench space of the sensor. Spearman rank correlations were assigned to each electrode for each force (Fig. 6). Spearman correlations have the ability to encode monotonic, non-linear correlations more faithfully than standard linear (Pearson) correlations. Only those electrodes that had a Spearman coefficient of > 0.1 were passed to the MLA.

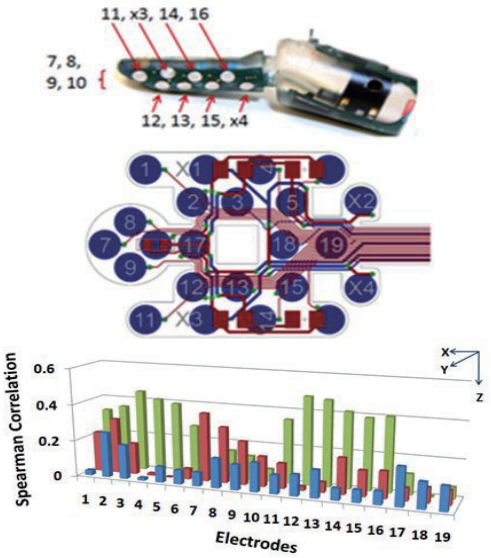


Figure 6: Top) Photograph of sensor showing numerical electrode assignments Middle) Splayed flex-circuit diagram showing all electrodes Bottom) Absolute Spearman correlations for all electrodes. Normal (Z) forces are represented in blue, front; tangential forces are in red (X; axial) and green (Y; lateral).

*D3. Sensory Data Integration*

In the previous paragraphs we have outlined how to extract ROC and PAF. We have also outlined several preprocessing and feature extraction techniques. The question remains which shall be implemented and in what order to achieve the best representation of forces from the BioTac? Here we examine the granularity ROC and PAF estimates and how this should be passed to a MLA to achieve the best generalization. The most straightforward method trains separate MLA's based on ROC and PAF data. We know that the sensor's response depends on these variables [8], so different MLAs should be trained based on these input classes. Two test sets were made to inspect radius of curvature; separate MLAs were generated for probes that engaged a small number of electrodes at high forces (1 and 3.6mm probe) and a relatively large number of electrodes at high forces (10mm and flat probe). These MLA's errors were then compared against an MLA that had been generated using all ROC data. Similarly, two test sets were made based on PAF. Near d =14mm, the BioTac begins to curve and taper, which will affect the manner in which forces deform the skin. Any percept with a d >= 14mm, was passed to a "forward" MLA and those with less to a "rear" MLA. Optimal spatial granularity remains to be determined.

After appropriate MLAs had been assigned based on ROC and PAF data, the appropriate preprocessing and feature extraction techniques were applied to the data sets. Five-fold cross validation was performed on each of the sets to check how well they generalized over randomly generated test sets for each force. RMSE, SMSE, R-squared and Percent Error (Eqn. 6) were reported where appropriate (integral evaluated numerically using the trapezoidal rule):

$$Error = 100\% \; x \int \frac{\sqrt{(Xpred - Xactual)^2}}{Xactual} \qquad (6)$$

## III. Results

### A. Radius of Curvature

A confusion matrix for the four-probe classifier is presented below (Fig. 7). The overall correct classification rate was 94.7%. The classifier performed as adequately in that smaller probes were less likely to be confused with larger probes; the flat probe produced the worst performance by far.

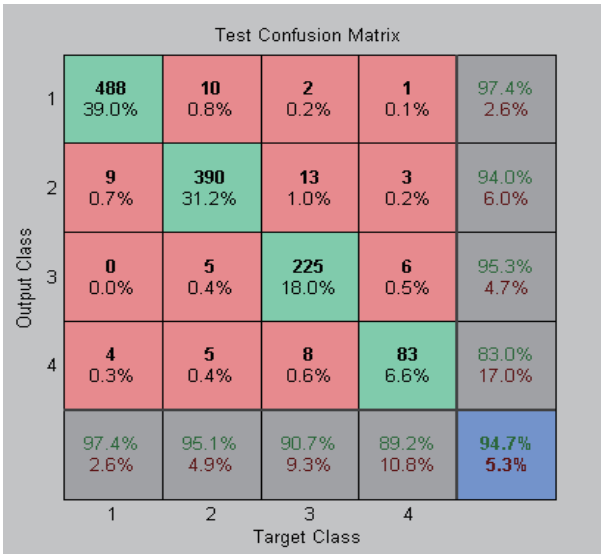


Figure 7: ANN classifier confusion matrix: Target classes 1-4 represent increasing ROC (1mm, 3.6mm, 10mm and flat probes. Green blocks show number and percent class samples in the data set, red blocks show misclassifications (false positives in the upper right, false negatives in the lower left); instances are listed on top (bold) and percentages below. Grey blocks show total classification percentages for each false positive/ negative row/ column and blue block shows average classification rate.

### B. Point of Application of Force

Fig. 8 shows the initial attempt at PAF discrimination.

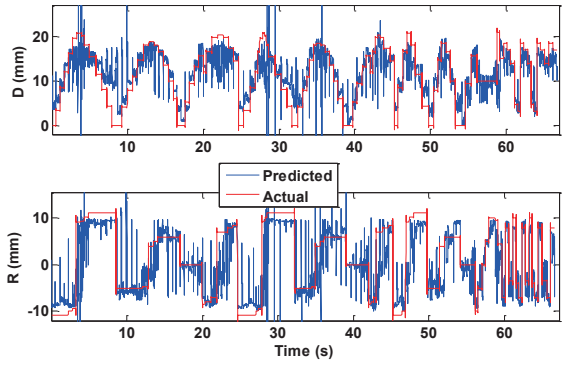


Figure 8: Predicted (blue) versus actual surface locations (red) Top) Distance approximation (blue); Bottom) Radial

The signal grossly matches the outline of the actual positions of the probes on the sensor but is very noisy. The likely cause of the signal "jumping" is contact at low force values. There are several force stimuli at the same position, so while the actual PAF remains constant over certain instances, the predicted position varies wildly at times due to the "divide by zero" problem in the calculation when there are little or no forces. To mitigate this, a dummy term could be replaced in the force equation to prevent the divide by zero problems, selective filtering/ smoothing could be performed or the algorithm could only be triggered above a certain threshold. Here we opt for the latter two. Another strategy is to perform the algorithm only above an estimated force threshold, as calculated by eqn. 1. Fig. 9 shows how results improve greatly when Lowess filtering is used. Statistics for

these plots and > 1N "Force Thresholding" are presented in Table 2.

Table 3: Statistics for PAF predictions

| Technique | RMSE | SMSE | $R^2$ |
|---|---|---|---|
| 11-pt Lowess – D | 3.19 | 0.244 | 0.782 |
| 11-pt Lowess – R | 3.50 | 0.218 | 0.802 |
| Force Thresholding – D | 2.37 | 0.183 | 0.839 |
| Force Thresholding – R | 2.90 | 0.198 | 0.813 |
| Both – D | 2.36 | 0.182 | 0.839 |
| Both – R | 2.89 | 0.197 | 0.813 |

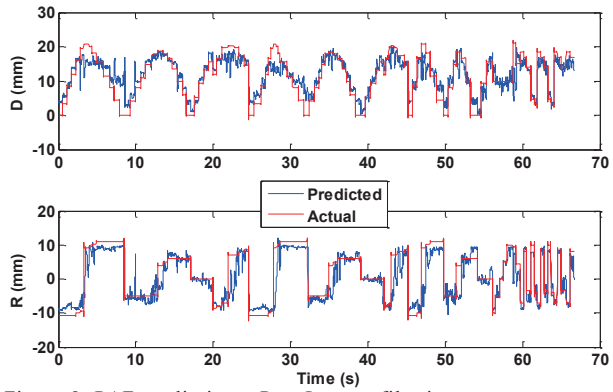


Figure 9: PAF prediction – Post Lowess filtering

While "force thresholding" has the drawback of clipping the working range of the sensor for PAF prediction, it provides RMSE discrimination on par with human fingertips. If the full working range is more important than accuracy, Lowess filtering can be used.

## C. Force Vector

### C1. Feature Extraction/ Dimensionality Reduction

Feature extraction techniques improved the performance of MLAs when averaged (Large ROC, Small ROC, Forward PAF, Rear PAF) over all measured (Fig. 10).

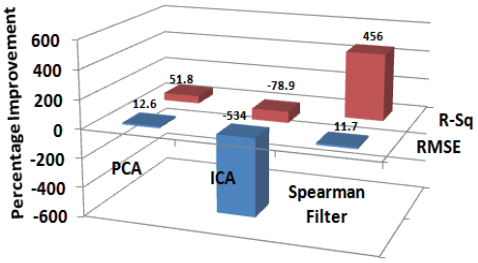


Figure 10: Feature extraction percentage improvements in RMSE and R2 across all forces and MLAs. $R^2$ shows a large percentage improvement due to the low original $R^2$ values for X-forces

Overall, the only notably poor performing feature extraction method was ICA. PCA resulted in modest increases in performance. The supervised feature extraction techniques need to be considered within the context of their individual forces. For the Spearman filter, Y- and Z-force performance increased the most, but not X. This is likely due to the small number of electrodes that would be sensitive to tangential forces in this axis (see coordinate frame, Fig. 6).

### C2. Sensory Data Integration

Fig. 11 shows the generalization improvement when MLAs are trained on data specific to location and ROC rather than a single "all-purpose" MLA. For example, the small and large ROC bars show percentage improvement when the data sets are divided and only trained and tested on small or large ROC probes. It should be noted that the ROC and PAF data passed to the MLAs were known *a priori*; they were not generated by the ROC classifier or the PAF processor. This was done to analyze independent performance. The effects of using the "wrong" secondary classifier based on an error in the primary classification are considered in the Discussion.

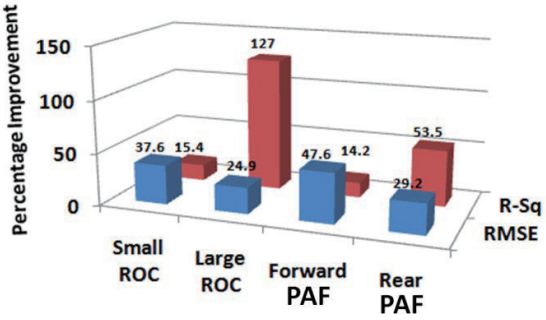


Figure 11: Improvements in RMSE and $R^2$ averaged across all forces and MLAs after segregating by ROC and PAF.

Table 2 shows a summary of 5-cross fold generalization error for a single ANN. To provide visualization, a typical generalization set across three forces is presented below for the "Large ROC-Rear PAF" for an ANN.

Table 4: Statistical metrics for set: "Rear-large ROC" MLA

| Force (Z) | | Force (Y) | | Force (X) | |
|---|---|---|---|---|---|
| $R^2$ | Error | $R^2$ | Error | $R^2$ | Error |
| 0.729 +/- .0282 | 31.4 +/- 1.86 | 0.931 +/- .0139 | 13.9 +/- 1.08 | 0.870 +/- .0603 | 37.9 +/- 7.24 |

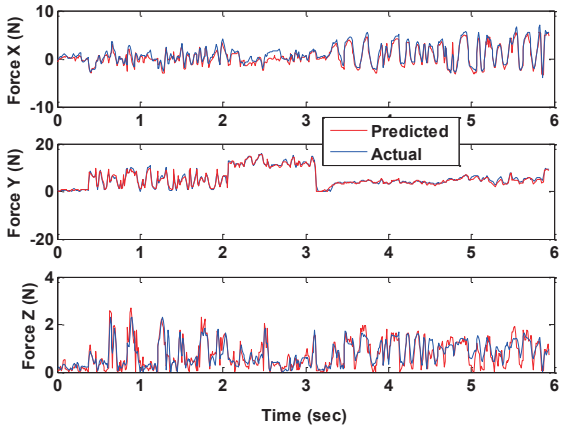


Figure 12: Tri-graph of forces versus ANN predictions over a representative generalization test of "rear-large ROC" data.

## IV. Discussion

### A. Radius of Curvature

As shown in Figure 7, overall correct classification rate is 94.7%. Smaller probes were less likely to be confused with larger probes. The flat probe produced the worst performance by far. The likely explanation for this is that the flat probe data set was sparser than the other probe sets. This would cause classification biasing towards the other sets; repeated probe movements to equalize the set numbers would remedy this. Overall performance might be improved by implementing feature extraction or force-thresholding to deal with poor performance at low force levels, similar to the PAF problem. Anecdotally, one can perform a self-experiment on discriminating object ROC with the human fingertip. As more sensory data become available at higher forces, the discrimination problem becomes simpler.

Optimizing ROC classification will require attention to the exploratory movements, which were not a controlled variable in this study. Based on collected data, it is difficult to compare the BioTac to human performance, which is usually reported as just-noticeable-difference (JND) between stimuli rather than the absolute classification reported here. In an experiment by Hannaford & Dosher [17], subjects reported a JND of ball diameter (12.69mm) between 2.3% and 4.7% of ball diameter. Provancher *et al.* [18] also report JND diameters of 1.68, 2.98, 8.00 and 11.48mm for 20, 40, 60 and 80mm diameter spheres respectively; JND percentages range from 8.4 to 14.3%. The smallest discrimination for the BioTac is between 1 and 3.2mm ROC probes, but this occurs at 98.5% accuracy, much higher than the 75% of JND. To properly compare human and BioTac performance, the BioTac would need to be stimulated with probes of much more granular nature, centered on probe values of regular interval.

### B. Point of Application of Force

PAF discrimination by interpolative look-up table proved promising yet problematic due to lack of discriminability at low force levels (leading to high "divide by zero" errors). To compensate, two different methods were examined. Lowess filtering offered the advantage of incorporating all data with an 11-sample delay. Force thresholding was more effective, achieving near-human discrimination levels (2 - 4mm for 2-pt discrimination; see also [19]) but at the cost of reducing usable dynamic range. A combination of the two methods yielded little increase in performance above force thresholding. This is likely due to the lack of noisiness in the look-up table method above a high threshold. Given the signal processing options and the error presented in both manually measuring, marking and applying forces as well as lateral drift of the probe in off-axis application of force, PAF determination seems relatively acceptable. Filtering has a guaranteed cost of a fixed sample delay (11 samples here). The threshold force used here (1.0N) was selected somewhat arbitrarily based on data from the 1mm ROC probe. A more biomimetic strategy might be to use all available cues to gradually improve estimation of PAF for a range of exploratory movements and forces. This is not unlike how humans use non-spatial cues such as varying force intensity (versus our fixed 1.0N threshold) to achieve finer discrimination at the fingertips (~1mm grating period, [20]).

### C. Force Vector

#### C1. Feature Extraction/ Dimensionality Reduction

For unsupervised feature detection, PCA greatly outperformed ICA, indicating that the features of interest must be uncorrelated to yield useful results. This makes sense intuitively as the conductance seen by an individual electrode tends to be dominated by the compression of the overlying skin against it. Some of the electrodes are oriented orthogonal to one another; therefore variance in one set of electrodes could be uncorrelated to another orthogonal set, suggesting that PCA is the appropriate tool to use. Regarding supervised feature detection, the Spearman filter seems to increase generalization performance. This is sensible, as non-correlated electrodes are removed from the machine learning problem, leading to a more tractable solution.

#### C2. Sensory Event Integration

The force vector extraction incorporated knowledge about the ROC and PAF of the contacted object, then used processed voltage data (by supervised and unsupervised feature extraction techniques) to extract each FV. Fig. 13 depicts the type and flow of machine learning processing for the BioTac.

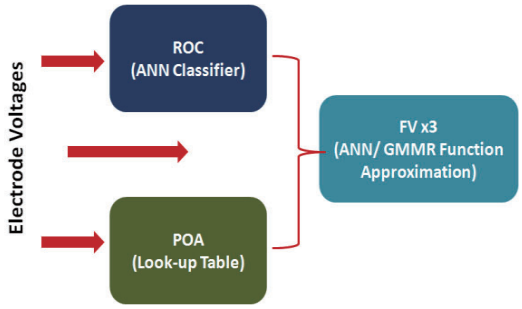


Figure 13: Illustration of information flow path for machine learning: classifier and look-up table simultaneously calculate ROC and PAF and pass this information to the function approximation for force along with sensor voltages

Four probe MLA classes were used to analyze the behavior of the sensor: "Forward-Small ROC,"(d>14mm PAF, 1 or 3.6mm probe) "Rear-Small ROC," (d<14mm PAF, 1 or 3.6mm probe) "Forward-Large-ROC" (d>14amm, 10mm or flat probe) and "Rear-Large ROC" (d<14mm, 10mm or flat probe). Generally, the MLAs for smaller ROC probes performed worse than for large ROC. This is sensible, as smaller ROC probes will engage fewer electrodes, giving the sensor less data to extract tri-axial forces. ANNs produced force errors (18-40%) that are worse, but similar to human force discrimination errors (6-9%) [21-22].

## V. CONCLUSION

We have shown that the BioTac encodes information required to extract the canonical representations of interactions with physical objects such as ROC, PAF and FV. The question remains whether it is necessary or useful to do so or whether the "raw" sensor signals should be used to solve haptic problems directly, as appears to occur in biological systems. The particle filter offers one possible tool to characterize sensor-object interactions. In addition to interpreting non-linear, non-Gaussian, multi-modal information, data from multiple sources (e.g. impedance sensors and vibration information) can be integrated into these structures during the resampling part of the algorithm. Grip state (X) (e.g. stable or slipping) and sensor measurement pairs ($Z_{1...n}$) can be assigned to support Bayesian architecture to estimate the posterior probability of the grip state:

$$P(Xt|Z1:t-1) = \int P(Xt|Xt-1)\,P(Xt-1|Z1:t-1)dXt-1 \quad (7)$$

Histograms and look-up tables can be developed to associate sensor values (from all available sensors) with various grip states during training. The particle filter then returns the mean of the particle likelihoods to yield the expected grip state. The output of such a trained particle filter can be used to modify the servo-control gains for a mechatronic hand, for example.

Such a particle filter was successfully implemented by Platt *et al.* [24] to localize a bump on a flexible surface using the uncalibrated tactile sensors of the Robonaut 2 system. In addition to localization and grip state estimation, particle filtering could also present solutions to tri-axial force representation. In principle, it could incorporate information acquired over time regarding the nature of the object and its dynamical interactions with the hand and its various sensors, improving the robustness of both object characterization and control.

The biomimetic fingertip and signal processing strategies presented in this work will not by themselves solve any of the above problems of object manipulation and identification. It does, however, provide a mechanically robust and informatically rich set of sensors that bears some resemblance to biological tactile sensors. Most of the tools and tasks of an industrial world were designed by humans to be performed by human hands in unstructured environments. This motivates the strategy of biomimetic design for prosthetic hands and robotic manipulators intended to function in this world.

## REFERENCES


[1] Wettels, N. Fishel, J.A., Su, Z. Lin, C.H and Loeb, G.E. "Multi-modal Synergistic Tactile Sensing" Tactile Sensing in Humanoids – Tactile Sensors and Beyond Workshop 9th IEEE-RAS International Conference on Humanoid Robots. Dec 7-10, 2009

[2] Puchhammer G., The tactile slip sensor: Integration of a miniaturized sensory device on a myoelectric hand. In Orthopädie-Technik Quarterly, English, edition I/2000:7-12, 2000.

[3] Wettels N., Parnandi A. R., Moon J. H., Loeb G. E, Sukhatme G. S., "Grip Control Using Biomimetic Tactile Sensing Systems", IEEE/ASME Transactions on Mechatronics: Focused Section on Anthropomorphism in Mechatronic Systems Vol. 14 No. 6, pp. 718-723 December 2009

[4] Evans M.H., Fox C.W., Pearson M.J., Prescott T.J. "Tactile discrimination using template classifiers: Towards a model of feature extraction in mammalian vibrissal systems" *From Animals to Animats 11 : Lecture Notes in Computer Science*, 2010

[5] Brett P. N. and Li Z. "A tactile sensing surface for artificial neural network based automatic recognition of the contact force position" *Proceedings of the Institution of Mechanical Engineers, Part I: Journal of Systems and Control Engineering* Vol 214 No 3 207-215, 2000

[6] Guo B. and Qin L. "Tactile Sensor Signal Processing with Artificial Neural Networks" *Advances in Intelligent and Soft Computing,* Volume 54, pp. 54-62, 2009

[7] Schneider, A., Sturm, J., Stachniss, C., Reisert, M., Burkhardt, H. and Burgard, W. "Object identification with tactile sensors using bag-of-features*." IEEE/RSJ International Conference on Intelligent Robots and Systems.* pp.43-48 St. Louis, MO USA 2009

[8] Wettels N., Santos V. J., Johansson R. S, and Loeb G. E., "Biomimetic tactile sensor array." *Advanced Robotics*, vol. 22, no. 7 pp. 829–849, June 2008

[9] Canepa G., Orazio S., De Rossi D. "Extraction of Cutaneous Primitives from Tactile Sensor Images" in *Proc of IEEE International Conf. on Systems, Man and Cybernetics* Vol. 3 pp. 2641-2646 San Antonio Tx USA, 1994

[10] Thint M. and Wang P.P. "Feature extraction and clustering of tactile impressions with connectionist models" In *Proc of International Conf. on Machine Learning* San Francisco, CA, USA 1990

[11] Allen, P. K. "Integrating vision and touch for object recognition tasks" *Int. J. Rob. Res.* Vol. 7 No. 6 pp. 15-33, 1988

[12] Johan T. and Wikander J. "Tactile sensing in intelligent robotic manipulation: a review" *Industrial Robot: An International Journal* Vol. 32 pp. 64-70, 2005

[13] Bishop C.M. Neural Networks for Pattern Recognition, Oxford: University Press, 1995

[14] Sarle, W.S. "Stopped Training and Other Remedies for Overfitting," Proceedings of the 27th Symposium on the Interface of Computing Science and Statistics, 352-360, 1995.

[15] Wettels, N. "Biomimetic Tactile Sensor for Object Identification and Grip Control" Dissertation at University of Southern California, May 2011.

[16] Hyvärinen, A. "Fast and Robust Fixed-Point Algorithms for Independent Component Analysis" *IEEE Trans. on Neural Networks,* 10(3):626-634, 1999.

[17] Hannaford, B. and Dosher J., Haptic Exploration of Spheres, *IEEE Haptics Symposium* Waltham, MA March 2010

[18] Provancher, W., Kuchenbecker, K., Niemeyer, G., and Cutkosky M.R. Contact Location Display for Haptic Perception of Curvature and Object Motion *International Journal of Robotics Research* Vol. 24 (9), September 2005

[19] Weinstein S. Intensive and extensive aspects of tactile sensitivity as a function of body part, sex and laterality, *The Skin Senses* Kenalsho (Ed.) pp. 195-222 Springfield, IL 1968

[20] Vega-Burmudez, F. and Johnson, K.O. Differences in spatial acuity between digits *Neurology 56* pp.1389-91, 2001

[21] Jones L. A. Perception and control of finger forces. In Proc. ASME Dynamic Systems and Control Division, pages 133–137,1998.

[22] Allin S., Matsuoka Y., and Klatzky R. Measuring just noticeable differences for haptic force feedback: Implications for rehabilitation.In Proc. 10th Symposium on Haptic Interfaces for Virtual Environments and Teleoperator Systems, pages 299–302, 2002.

[23] Platt, R., Permenter, F and Pfieffer, J. "Using Bayesian Filtering to Localize Flexible Materials During Manipulation" *IEEE Transactions on Robotics, Vol. 27, No. 3, June 2011*